Development 135, 3765-3774 (2008) doi:10.1242/dev.024034

Retinoic acid and Cyp26b1 are critical regulators of osteogenesis in the axial skeleton

Kirsten M. Spoorendonk[1], Josi Peterson-Maduro[1], Jörg Renn[2], Torsten Trowe[3], Sander Kranenbarg[4], Christoph Winkler[2] and Stefan Schulte-Merker[1,*]

Retinoic acid (RA) plays important roles in diverse biological processes ranging from germ cell specification to limb patterning. RA ultimately exerts its effect in the nucleus, but how RA levels are being generated and maintained locally is less clear. Here, we have analyzed the zebrafish *stocksteif* mutant, which exhibits severe over-ossification of the entire vertebral column. *stocksteif* encodes *cyp26b1*, a cytochrome P450 member that metabolizes RA. The mutant is completely phenocopied by treating 4 dpf wild-type embryos with either RA or the pharmacological Cyp26 blocker R115866, thus identifying a previously unappreciated role for RA and *cyp26b1* in osteogenesis of the vertebral column. *Cyp26b1* is expressed within osteoblast cells, demonstrating that RA levels within these cells need to be tightly controlled. Furthermore, we have examined the effect of RA on osteoblasts in vivo. As numbers of osteoblasts do not change upon RA treatment, we suggest that RA causes increased activity of axial osteoblasts, ultimately resulting in defective skeletogenesis.

KEY WORDS: Cyp26b1, Osteoblast, Osteogenesis, Retinoic acid, Zebrafish

INTRODUCTION

Retinoic acid (RA) has been demonstrated to play important roles in processes as diverse as cardiac specification (Keegan et al., 2005), patterning of both the central nervous system (Hernandez et al., 2007) and the tetrapod limb (Yashiro et al., 2004), as well as specification of germ cell fate (Bowles et al., 2006). RA is synthesized intracellularly from its precursor, vitamin A (or retinol), by retinaldehyde dehydrogenases (Raldhs) and transported to the nucleus where it initiates transcription of target genes (Ross et al., 2000; Maden, 2002). Levels of RA are determined by Raldhs and, in addition, by Cyp26 enzymes, members of the RA catabolizing cytochrome P450 family (White et al., 2000; MacLean et al., 2001). In vertebrates, three Cyp26 enzymes have been identified: Cyp26a1, Cyp26b1 and Cyp26c1 (White et al., 1996; Nelson 1999; Gu et al., 2005).

In mice, a *Cyp26a1* knockout that exhibits spina bifida and tail truncation as a consequence of patterning defects, and also shows homeotic transformations of anterior vertebrae has been described (Abu-Abed et al., 2001; Sakai et al., 2001), whereas *Cyp26b1* knockout mouse embryos display craniofacial defects and reduced limbs (Yashiro et al., 2004). Homozygous mutants die immediately after birth owing to respiratory distress before vertebral defects become obvious, and hence no other bone defects have been reported. In zebrafish, the effects of Cyp26 enzymes have been studied in the context of hindbrain (Emoto et al., 2005; Hernandez et al., 2007; White et al., 2007) and neural crest patterning (Reijntjes et al., 2007).

In this study, we have characterized a zebrafish mutant in *cyp26b1*, which exhibits severe over-ossification of the vertebral column. In both zebrafish and mouse, we report expression of *cyp26b1* in osteoblasts of the pre-vertebrae regions. We suggest that it is the tight regulation of RA within osteoblasts by Cyp26b1 activity that is crucial for axial osteogenesis.

In zebrafish and medaka, which are considered to have highly similar modes of axial skeleton ossification (Inohaya et al., 2007), vertebrae form by intramembranous ossification without passing through a cartilage stage (Ekanayake and Hall, 1987; Fleming et al., 2004). It has been suggested for both species that notochord cells are involved in the initial bone matrix formation of the centra during development of the vertebral column (Fleming et al., 2004; Inohaya et al., 2007). However, Inohaya et al. (Inohaya et al., 2007) could also show that sclerotome-derived progenitor cells differentiate into osteoblasts on the surface of the notochordal sheath, where they produce and mineralize bone matrix: this matrix is formed by cells distal to the notochord. Subsequent vertebral growth then proceeds from the anterior and posterior edges of the forming centra.

Until now, several in vitro studies have reported effects of RA exposure on mineralization, however, with contradicting results. Some studies describe an increase in mineralization (Skillington et al., 2002; Wang and Kirsch, 2002; Song et al., 2005; Yamashita et al., 2005; Malladi et al., 2006; Wan et al., 2007), whereas others report a suppression of cell differentiation and therefore a decrease in mineralization (Cohen-Tanugi and Forest, 1998; Iba et al., 2001) upon RA treatment of cultured cells. Here, we establish an in vivo model to follow early osteoblasts. We show that, upon RA treatment, axial osteoblasts in *osterix:nuGFP* transgenic zebrafish retain their normal positions. Moreover, osteoblast numbers do not change. Therefore, over-ossification of the axial skeleton upon RA excess is most probably caused by increased activity of osteoblasts along the vertebral column.

MATERIALS AND METHODS

Transgenic *osterix:mCherry* and *osterix:nuGFP* zebrafish

A 4.1 kb upstream regulatory region of the medaka *osterix* gene was amplified using the primers 5′-TGAACATGTCAGTGCCATCA-3′ (forward) and 5′-CGGGACAGTTTGGAAGAAGT-3′ (reverse) and cloned in front of mCherry. Transgenic zebrafish were generated by injection into one-cell stage embryos using the I-*Sce*I meganuclease approach (Rembold et al., 2006). The same upstream region was cloned in front of a nuclear

[1]Hubrecht Institute, KNAW & University Medical Centre Utrecht, 3584 CT Utrecht, The Netherlands. [2]Department of Biological Sciences, National University of Singapore, 117543 Singapore. [3]Exelixis, San Francisco, CA, USA. [4]Wageningen University, Experimental Zoology Group, 6709 PG Wageningen, The Netherlands.

*Author for correspondence (e-mail: s.schulte@niob.knaw.nl)

Accepted 15 September 2008

localization signal followed by GFP (nuGFP), and transgenic zebrafish were generated using the Tol2 transposon system (Kawakami et al., 1998). Cloning details are available upon request.

BAC recombineering

YFP was recombined directly after the ATG site of the gene of interest on a BAC clone, containing the genomic information of the gene of interest (Kimura et al., 2006). The following BACs and primers were used: DKEY-53014 (containing 73.5 kb upstream of the *cyp26b1* coding region, and >73.5 kb downstream of *cyp26b1*); Cyp26b1_GFP_fw (ttgctcatcactccaa-agagatatttgagacaagtccccggacgttcacaACCATGGTGAGCAAGGGCGAGG AG); Cyp26b1_Neo_rev (cacgcagccagcgtcgccaacgccgagacaaggtcaaaactctc-gaagagTCAGAAGAACTCGTCAAGAAGGCG); and CH211-51D23 (containing 111.6 kb upstream of the *osx*-coding region, and 66.3 kb downstream of *osx*); Osx_GFP_fw (cagctctcctctcccgcttttggattgacc-ctcactggactgcttcctccACCATGGTGAGCAAGGGCGAGGAG); and Osx_Neo_rev (gcagctgtgagatcgcagtgagttttccgtacctccagaatcgacgcggcTCA-GAAGAACTCGTCAAGAAGGCG).

Meiotic mapping

The *stocksteif* mutation was mapped to linkage group 7 using standard simple sequence length polymorphism mapping. The following six primers were used for fine mapping: R3.2-fw (5′ ACCGTAATTGAAACCACGTC 3′), R3.2-rv (5′ GCCAAATATTTCGATCTGTG 3′), R1.11-fw (5′ GATGCTCAGACCTGTGTTTG 3′), R1.11-rv (5′ TGAAGTCAATG-CTGGTCAAC 3′), R2.22-fw (5′ TCACCCTTCCATGAACTTAAC 3′) and R2.22-rv (5′ AAACAGCCAGCGTAGATAAAC 3′).

Skeletal staining

Embryos were fixed in 3.5% formaldehyde/0.1 M sodium phosphate buffer for 1 hour and stored in 70% methanol. The protocol for simultaneous bone and cartilage staining was adapted from that previously described (Walker and Kimmel, 2007). Briefly, embryos were rinsed in 50% ethanol and subsequently stained with 0.2 mg/ml Alcian Blue 8 GX (Sigma) in 70% ethanol/80 mM $MgCl_2$. After washes in 0.02% Triton, embryos were bleached in 1% H_2O_2/1% KOH for 30 minutes, washed in a saturated sodium tetraborate solution, and digested for 1 hour in 1 mg/ml trypsin (Sigma) in 60% saturated sodiumtetraborate. Bones were stained with 0.04 mg/ml Alizarin red S (Sigma) in 1% KOH. Destaining was carried out in an increasing glycerol series (10%, 30%, 70%) and specimens were stored at 4°C in 70% glycerol.

For Alizarin Red staining only, the Alcian Blue step was omitted. Juvenile fish were fixed for 2 hours, incubated in acetone to remove fat (up to 24 hours) and digested with 10 mg/ml trypsin in 60% sodiumtetraborate overnight. Scales were removed manually. In vivo skeletal staining was carried out with 0.001% calcein (Sigma) in embryo water for at least 2 days.

Pharmacological treatments

Stock solutions of 10 mM all-trans retinoic acid (Sigma) and 10 mM R115866 (Janssen Pharmaceutica) in DMSO were diluted in embryo medium. Sibling controls were incubated in corresponding dilutions of DMSO. RA treatments were carried out in the dark and solutions were changed every ~12 hours.

MicroCT scans

Fixed samples were wrapped in parafilm and scanned with a Skyscan 1072 microCT system at 80 kV and 100 μA. The cubic voxelsize was 6.08 μm for the wild type and 2.73 μm for the *stocksteif* animals. The scans were reconstructed and subsequently segmented as previously described (Feldkamp et al., 1984; Waarsing et al., 2004). The segmented images were visualized as a surface using a custom-written Matlab 7.3 script.

In situ hybridization

For all sectioned zebrafish material, in situ hybridization was carried out first on whole-mount embryos (Schulte-Merker, 2002), and only subsequently were embryos embedded in 3% agarose and cut (100 μm sections) on a vibrotome (Microm HM650V), or embedded in plastic and cut (10 μm sections) on a microtome (Leica RM2035). For sections of mouse material, paraffin-embedded embryos were sectioned then hybridized in situ, according to standard procedures (Moorman et al., 2001).

RESULTS

In a screen for genes that affect ossification in zebrafish, we identified a single allele of the *stocksteif* mutant, sst^{t24295}. Mutant embryos are characterized by an early onset over-ossification of the notochord, resulting in fused vertebral centra (Fig. 1A). In this original allele, *sst* mutants are comparable in size and external features with their wild-type siblings, and therefore the phenotype can be detected only by skeletal staining at 8 days post fertilization (dpf) or later. Skeletal staining of siblings shows an equidistant distribution of vertebrae along the notochord, whereas in mutants most of the vertebrae are fused. Examining mutants that were not completely synchronous enabled us to conclude that initially centra are placed in a proper pattern along the notochord, but that later the excess of developing bone causes fusion of the vertebrae (insets in Fig. 1A).

To assess whether the phenotypic effects might be due to early patterning defects, we performed in situ hybridization for somitic markers (*myoD*, *smad1*), which did not show any differences between mutants and siblings (data not shown).

In a few exceptional cases, mutants survived when separated early from their siblings, until a maximum age of 6 months. These mutants remain smaller (Fig. 1B), have problems swimming and exhibit a protruding jaw (Fig. 1C). In skeletal preparations, most centra appear fused, and only about five distinct intervertebral boundaries can be observed along the body axis (Fig. 1C). Neural and haemal arches both exhibit fan-shaped expansions (Fig. 1C). Furthermore, the angles of the arches with respect to the body axis are more irregular and obtuse in mutants than in siblings. The phenotype is not restricted to the vertebral column at this later stage: hypurals partially fuse in the tail, and the head skeleton shows abnormalitites as well (Fig. 1C). Phenotypic analysis of 3-, 6- and 9-week-old mutants showed that the severity of bone defects increases over time with the older mutants exhibiting the broadest arches (data not shown).

MicroCT scans demonstrate that in *sst* mutants excess bone can replace the notochord by proximal growth, leading to completely solid centra (Fig. 1D), whereas the notochord remains present as a continuous rod in the vertebral column of wild-type siblings (see Fig. S1 and S2 in the supplementary material).

stocksteif encodes *cyp26b1*

In order to molecularly identify the *stocksteif* locus, we positionally cloned the gene. The mutation mapped to linkage group 7 (Fig. 2A). Fine mapping identified two flanking markers on BAC clone zC197C14. In 839 embryos tested, R3.2 left two recombinants (<0.2 cM) and R1.11 left one recombinant (<0.1 cM). The single gene enclosed by both markers is *cyp26b1*. Sequence analysis of the coding region of *cyp26b1*, as well as exon-intron-boundaries revealed no mutations causing amino acid alterations. Indeed, the sequence of mutant *cyp26b1* cDNA also showed no base changes.

To obtain additional alleles of *sst*, we performed a reverse genetic screen (Wienholds et al., 2002). One allele, a nonsense mutation in exon 1, is predicted to change a lysine to a stop codon at position 46 (K46STOP; sst^{sa0002}) out of 512 amino acids in the putative wild-type protein. Another allele, a splice donor mutation (sst^{sa0003}), changes the most 5′ nucleotide of intron 2 from G to A (Fig. 2B), probably resulting in deficient splicing of this intron and consequently a full knockout of the encoded protein. Fig. 2C,D show Alizarin Red stained progeny from a cross between the two original sst^{sa0002} and sst^{sa0003} founders. Identical stainings were also obtained for transheterozygous embryos from crosses between sst^{sa0002} and sst^{t24295} carriers, and homozygous mutant embryos for both newly obtained alleles, sst^{sa0002} and sst^{sa0003} (data not shown).

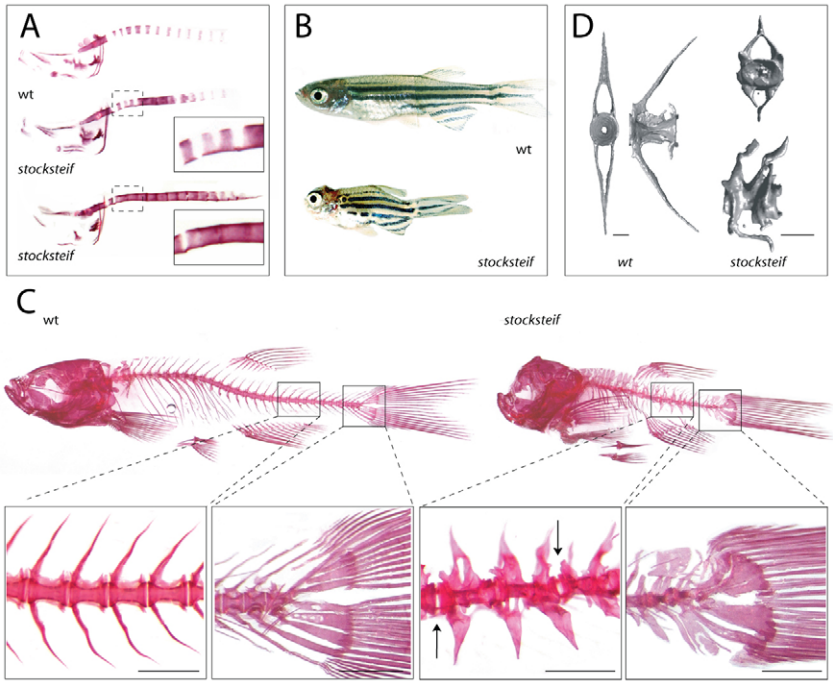

Fig. 1. *stocksteif* mutants exhibit over-ossification of the larval and adult vertebral column. (**A**) Alizarin Red bone staining of a wild-type embryo and two *stocksteif* embryos at 8 dpf. Insets show that the initial spacing of vertebrae is normal (upper inset), but that excessive bone formation causes fusion of the future vertebrae (both insets). (**B**) Sibling wild-type and *stocksteif* juveniles (2 months). Pictures are taken at the same magnification. (**C**) Alizarin Red bone staining of wild-type and *stocksteif* juveniles (2 months) shown to scale with magnifications of part of the vertebral column and the tail. In mutants, vertebrae are usually fused with each other, and only few intervertebral boundaries can be observed (arrows). Hypural elements in the tail are also fused. Note expansion of both neural and haemal arches in mutants. Scale bars: 500 μm. (**D**) MicroCT scans of wild-type (3 months) and *stocksteif* juveniles (2 months) show that mutants exhibit completely solid centra, with the central opening (area of the nucleus pulposus) completely filled by excess bone. Scale bars: 100 μm.

As described above, we have been able to raise a few homozygous mutants from the original sst^{t24295} allele. By contrast, all transheterozygous embryos (both $sst^{sa0002}/sst^{sa0003}$ and $sst^{sa0002}/sst^{t24295}$), as well as the homozygous embryos for sst^{sa0002} and sst^{sa0003} die around day 8 of development, without developing a swim bladder. In addition to the over-ossification of the vertebral column, these mutants also exhibit a protruding jaw and lack some tissue dorsal to the ethmoid plate (Fig. 2C′,D′,E-G). The cartilage derived ethmoid plate itself (asterisk in Fig. 2G) is reduced in size and shows a more narrow morphology in homozygous sst^{sa0002} and sst^{sa0003} mutants than in siblings.

However, mRNA expression of bone-specific markers such as type X collagen (*Col10a1*), shown to be expressed in intramembranous bone in zebrafish (Avaron et al., 2006) and *osterix*, a specific marker for mature osteoblasts (Nakashima et al., 2002) is not altered in mutants. In situ hybridizations for both markers at 4 dpf do not show any differences between siblings and mutants (Fig. 2H-K; see Fig. S3 in the supplementary material).

In situ hybridization for *cyp26b1* showed that expression levels in homozygous mutants are upregulated in comparison with siblings (see Fig. S4H,I in the supplementary material), suggesting a positive-feedback response to increased RA levels.

In summary, this shows that *cyp26b1* deficiency leads to cranial cartilage defects. By contrast, bone structures are not affected in the head at this stage, but show severe over-ossification in the trunk.

Cyp26b1 is expressed in osteoblasts

To further understand the role of Cyp26b1 in ossification, we examined its expression pattern both in zebrafish and mice. In zebrafish, we confirmed previously reported *cyp26b1* expression up to 72 hpf (Zhao et al., 2005) in the head region, covering expression in the hindbrain, branchial arches and pectoral fins (Fig. 3A, see Fig. S4A-C in the supplementary material). In addition, we here show that previously unreported expression can also be found in bone elements [examples are shown in Fig. 3A (cleithrum), Fig. S4E (operculum) and Fig. S4F,G in the supplementary material (parasphenoid)]. Moreover, we report a segmented pattern in the area surrounding the notochord that is most clearly visible in *sst* mutants because of their upregulated *cyp26b1* levels (Fig. 3B). To determine whether the latter staining represents expression in sclerotome-derived cells, we compared *cyp26b1* expression with that of *twist* (Fig. 3C,D), which has been shown to be specific, within the somites, for sclerotome in zebrafish (Morin-Kensicki and Eisen, 1997) as well as in medaka (Renn et al., 2006). Expression patterns of *cyp26b1* and *twist* do correspond with one another, indicating that *cyp26b1* in zebrafish is expressed in sclerotome-derived cells.

To investigate whether *cyp26b1* is expressed in osteoblasts, we first generated a new transgenic zebrafish reporter line, in which mCherry expression is controlled by the medaka *osterix* promoter (Renn and Winkler, unpublished). Briefly, in transgenic larvae, *osterix*:*mCherry*-positive cells in the head are seen in all intramembranous bones, such as parasphenoid and cleithrum, and later in the operculum and branchiostegal rays, as well as in endochondral bones (data not shown).

In order to compare *osterix* expression with *cyp26b1* expression in vivo, we recombined YFP into a BAC clone that contained the genomic sequence of *cyp26b1*. This construct was injected into one-cell stage *Tg(osx:mCherry)* embryos. Because in these transient assays not all cells will incorporate the *cyp26b1:YFP* construct, we expected patchy *cyp26b1:YFP* expression. Indeed, we were able to detect single YFP-positive cells in *osx:mCherry* positive bone elements (Fig. 3F-K). In various embryos that we have analyzed, we have only seen YFP expression in places where we had previously observed *cyp26b1* mRNA expression. Ectopic expression was never observed. We conclude that *cyp26b1* is expressed in osteoblasts.

In mice, *Cyp26b1* is expressed during early embryonic development in the hindbrain, neural tube, craniofacial structures, in outgrowing limb buds (MacLean et al., 2001) and in the pre-vertebrae regions at E12.5 and E14.5 (Abu-Abed et al., 2002). We confirm and extend these findings by showing that also in mice it is the condensing sclerotome surrounding the notochord that expresses *Cyp26b1* (Fig. 4B,C), as in zebrafish.

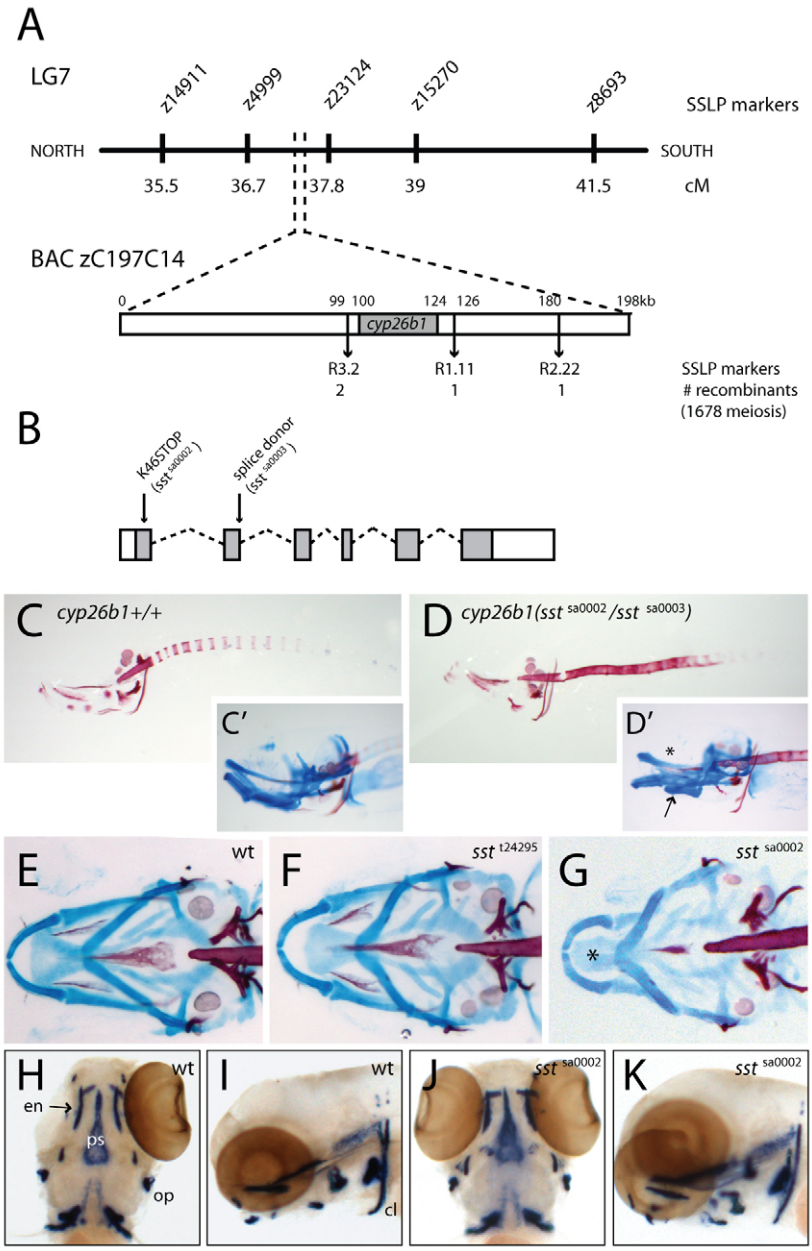

Fig. 2. *stocksteif* encodes *cyp26b1*. (**A**) *stocksteif* was mapped to a narrow region on linkage group 7. Flanking SSLP markers are both located on BAC zC197C14. *cyp26b1* appears to be the only gene present on the clone. (**B**) Schematic overview of *cyp26b1* structure on the genomic level with nonsense (K46STOP or sst^{sa0002}) and splice donor (sst^{sa0003}) mutation indicated. Translated parts of the exons are shaded. (**C**,**D**) Alizarin Red bone staining of a *cyp26b1*+/+ embryo and a transheterozygous *cyp26b1*(sst^{sa0002}/sst^{sa0003}) embryo. (C′,D′,E-G) Double staining with Alcian Blue for cartilage and Alizarin Red for bone. (**C′**,**D′**) A *cyp26b1*+/+ embryo shows normal cartilage, whereas a transheterozygous *cyp26b1*(sst^{sa0002}/sst^{sa0003}) embryo shows missing tissue dorsal to the ethmoid plate (asterisk) and fusion of the ceratohyal with the basihyal (arrow). (**E-G**) Ventral views of a wild-type embryo (E), a homozygous sst^{t24295} mutant (F) and a homozygous sst^{sa0002} mutant (G). Note the reduced and misshaped ethmoid plate (asterisk) in the sst^{sa0002} mutant. (**H-K**) Expression of *col10a1* is not changed in 4 dpf wild-type siblings (H,I) versus mutants (J,K). cl, cleithrum; en, entopterygoid; op, operculum; ps, parasphenoid.

Furthermore, in situ hybridizations on consecutive sections using probes against *Cyp26b1* and *Osterix* show expression of both genes in overlapping regions of the mouse axial skeleton (Fig. 4D-G). Vertebrae are formed in an anterior-posterior progression with more posterior vertebrae being less mature than anterior ones. *Cyp26b1* is expressed in all forming vertebrae, including the most posterior ones (arrows in Fig. 4D), whereas *Osterix* is expressed only in the most mature vertebrae (Fig. 4F). Thus, *Cyp26b1* expression precedes *Osterix* expression.

We conclude that, as in zebrafish, murine *Cyp26b1* is expressed in osteoblasts and that expression of *Cyp26b1* is conserved among vertebrates. The expression pattern of *cyp26b1* is consistent with the axial skeletogenesis phenotype in *stocksteif* mutants.

In vivo observations of axial *osterix* expression

In the course of these studies, we noticed that in zebrafish axial *osterix* expression could be detected only at points in time when neural and haemal arches were about to appear at day 17 (Fleming et al., 2004) (K.M.S. and S.S.-M., unpublished). We have failed to detect *osterix* mRNA in the axis prior to this point in time. This suggests that cells that form the calcified material of the centra do not express *osterix* at these stages in zebrafish.

Further support for this notion stems from the analysis of a transgenic zebrafish line, in which mCherry is controlled by the medaka *osterix* promoter. Here, we only detect mCherry-positive cells in the arches and at the anterior and posterior edges of the forming vertebrae, but not in the central part of the centra at this stage. Expression could be detected only shortly prior to the formation of neural and haemal arches (see Fig. 6A-D). To confirm that this is not a limitation of the transgene, we have recombined YFP into a BAC containing the zebrafish *osterix* gene. Again, after injections of this construct in one-cell stage embryos, we were able to detect expression only in cranial bone and, after day 17, in haemal and neural arches. The main bodies of the centra, however, were always devoid of YFP expression in these transient expression

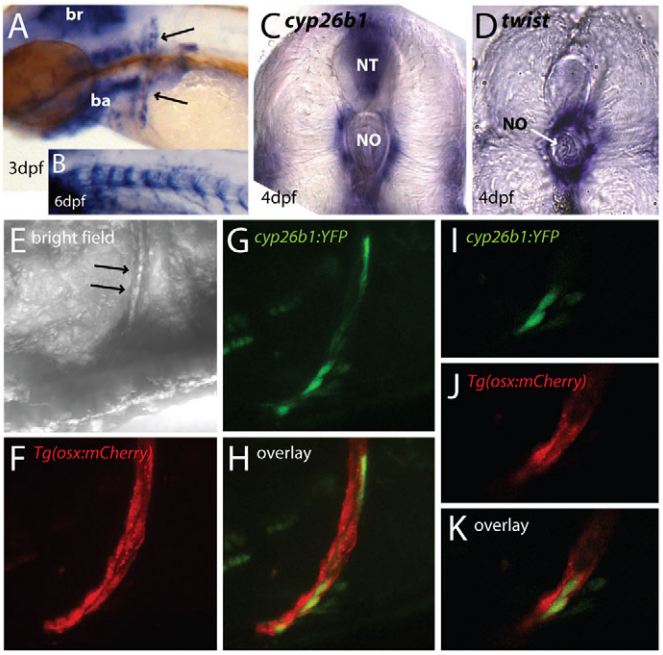

Fig. 3. *cyp26b1* is expressed in zebrafish osteoblasts. (A-C) *cyp26b1* expression in zebrafish. (**A**) Early *cyp26b1* expression in zebrafish is found in the hindbrain, branchial arches, pectoral fins and the cleithrum (arrows). (**B**) At 6 dpf, *cyp26b1* expression is seen in a segmented pattern around the notochord. A mutant embryo is shown, as *cyp26b1* mRNA levels are higher in mutants than wild-type embryos. (**C**,**D**) Vibratome transverse sections (4 dpf, 100 μm) showing *cyp26b1* expression (C) surrounding the notochord (no) and in the neural tube (nt), and expression of the sclerotome marker *twist* in cells juxtaposed to the notochord (D), similar to *cyp26b1* expression. (**E**) Bright-field view of an embryonic trunk with arrows indicating the cleithrum. (F-K) Co-localization of *cyp26b1:YFP* and *osx:mCherry* in osteoblasts of the cleithrum. (**F**) Cleithrum cells are labelled in *Tg(osx:mCherry)* embryos. (**G**,**H**) Transient expression of *cyp26b1:YFP* in cells of the cleithrum at 4 dpf, with projection in H demonstrating colocalization of both genes in the same cells. (**I-K**) Single confocal scans of a part of the projections shown in F-H. Anterior is towards the left, except where stated otherwise.

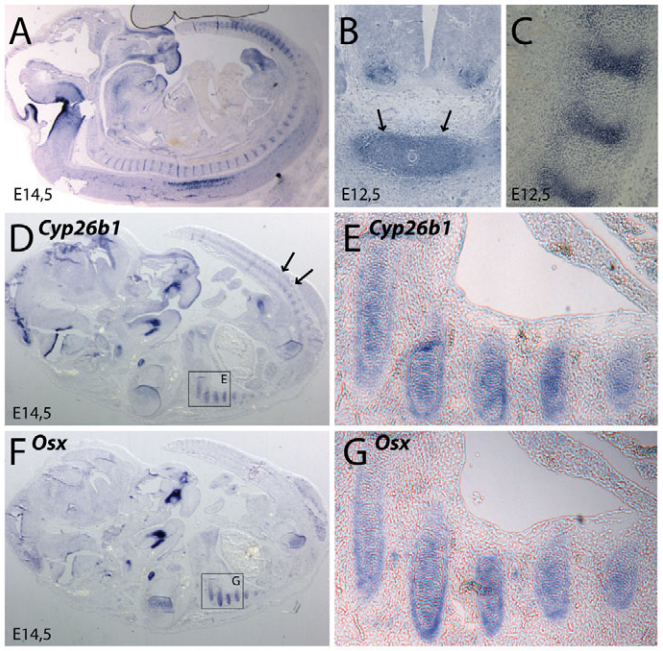

Fig. 4. *Cyp26b1* is expressed in mouse osteoblasts prior to osterix expression. (A-E) *Cyp26b1* expression in mice. (**A**) At E14.5 *Cyp26b1* mRNA is present in the brain, neural tube, craniofacial structures and in the pre-vertebrae regions. (**B**) Transversal section (E12.5) showing expression of *Cyp26b1* in the cells of the condensing sclerotome (arrows) around the notochord. (**C**) Detail of sagittal section (E12.5) confirming the segmented pattern in the pre-vertebrae regions. (**D-G**) Consecutive sections showing expression of *Cyp26b1* (D, enlargement in E) and osterix (F, enlargement in G) in the forming vertebrae. Expression is seen in exactly the same region, showing that *Cyp26b1* is expressed in osteoblasts. Arrows in D indicate expression of *Cyp26b1* in posterior vertebrae where osterix is not expressed yet.

assays (data not shown). Both transgenic lines show identical results and exhibit expression patterns identical to those we observe with *osterix* mRNA in situ.

We conclude that zebrafish *osterix* is very likely not expressed in cells that are responsible for early ossification of the centra. *osterix* expression, in the axial skeleton, is restricted to the anterior and posterior edges of the forming vertebrae, as well as to neural and haemal arches.

Treatment of wild-type embryos with either retinoic acid or R115866 phenocopies the *stocksteif* mutant phenotype

As *sst* mutants lack Cyp26b1 activity and therefore should have at least a local excess of RA, we asked whether RA treatment of wild-type embryos can phenocopy the mutant phenotype. Treatments were started at day 4 or later to avoid defects associated with early RA treatments of embryos (Keegan et al., 2005; Hernandez et al., 2007; Reijntjes et al., 2007). Wild-type embryos were treated with 1 μM RA starting at day 4, 5, 6 or 7 of development. At 8 dpf, Alizarin Red staining was performed. Sibling controls received equivalent treatments of DMSO, with no detectable effect on ossification. RA treatments, however, resulted in three phenotypic classes, all exhibiting axial over-ossification, with the most severe one completely mimicking the *sst* mutant phenotype (Fig. 5A). As shown in Fig. 5B, all embryos for which treatment was started at 4 dpf showed a phenotype, with 35% exhibiting a completely over-ossified notochord. For treatments started at 5 dpf and 6 dpf, respectively, 90% and 70% showed a phenotype. Embryos treated for 24 hours with RA onwards from day 7 were indistinguishable from controls, presumably as 24 hours were insufficient to allow for mineralization to occur.

To investigate more specifically the effect of aberrant Cyp26b1 function, we treated wild-type embryos with 0.5 μM of the R115866 compound, a selective antagonist for the three Cyp26 enzymes (Hernandez et al., 2007). Treatments were identical, and results near-identical to the described RA treatments: all embryos for which treatment was started at day 4 showed a phenotype resembling the *sst* mutant (Fig. 5C).

Osteoblast numbers do not alter upon retinoic acid treatment

Obvious explanations for the observed phenotype would be mislocalization of osteoblasts, an increased number of osteoblasts or increased osteoblast activity. In order to distinguish between these scenarios, and in order to quantify precisely osteoblasts in vivo, we

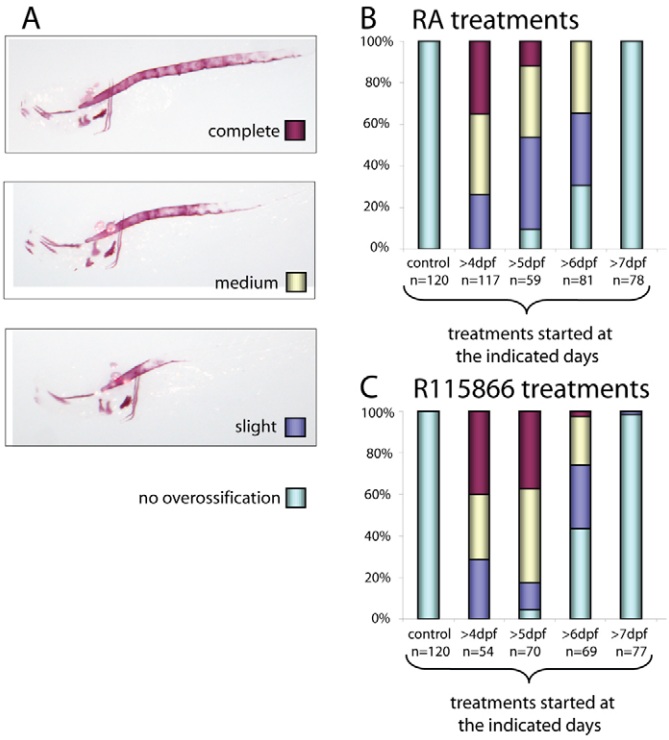

Fig. 5. Treatment of wild-type embryos with either retinoic acid or R115866 phenocopy the *stocksteif* mutant phenotype. (**A**) After treatment of wild-type embryos with 1 μM RA, three phenotypic classes were observed, with the most severe phenotype completely mimicking the *sst* mutant phenotype. (**B**) Results are shown for RA treatments that were started at the days indicated and continued until the embryos were fixed at 8 dpf. Control treatments with only DMSO were started at day 4. (**C**) Treatment of wild-type embryos with 0.5 μM R115866 resulted in the same three phenotypic classes as shown for the RA treatments in A.

established, next to the described *osterix:mCherry* line, an additional line with nuclear GFP (nuGFP) controlled by the medaka *osterix* promoter region. Unfortunately, because even the hypomorphic sst^{t24295} allele is near-lethal, we have not been able to obtain homozygous sst^{t24295} larvae in this transgenic background. Therefore, we decided to visualize directly the response of osteoblasts to excess RA in the *osterix:nuGFP* zebrafish line.

When zebrafish embryos are treated with 0.1 μM RA from 17 dpf to 20d pf, i.e. after onset of endogenous and transgenic *osterix* expression, over-ossification of the axial skeleton can be observed as evidenced by fusion of vertebrae (Alizarin Red bone staining in Fig. 6E-H), identical to our RA treatments described above (compare with Fig. 5A). The localization of GFP-positive osteoblasts in RA-treated embryos, however, is not altered in comparison with DMSO controls (compare Fig. 6I with 6L). In most treated cases, the space between centra was easily recognizable, even though anterior and posterior edges of centra were not delineated as straight as in DMSO control cases, probably owing to the large amount of ectopic bone matrix that is laid down in the spaces between the centra.

Next, we performed cell counts. Although in projections of confocal scans it is not always clear whether a spot of GFP expression refers to one or more nuclei, nuclei of separate cells can be clearly distinguished from each other in single confocal scans [e.g. the encircled spot in one projection (Fig. 6J) was resolved to represent two cells in a single scan (Fig. 6K)]. Furthermore, cells that are seen in projections but belong to arches at the other side of the embryo can be discriminated in single scans [examples of such cells are indicated with arrows in projections (Fig. 6J,M)]. Therefore, all cell counts were carried out in single confocal scans. In at least five different larvae per condition, several segments were counted (schematic representation of counted area is seen in Fig. 6O). As shown in Fig. 6P, there is no significant difference in numbers of *osterix:nuGFP*-positive cells between DMSO controls and RA-treated larvae. In conclusion, RA treatment of embryos from 17 to 20 dpf does not alter localization of mature *osterix*-expressing osteoblasts or their numbers.

DISCUSSION

The *stocksteif* mutant phenotype

In this study, we characterized the zebrafish mutant *stocksteif*, which exhibits severe over-ossification of the vertebral column. Initially, centra are placed in a wild-type pattern along the notochord, but later the excess of developing bone causes fusion of the vertebrae. This suggests that over-ossification in *sst* mutants is not due to a defect in initial anterior-posterior patterning, and is therefore distinct from the *fused somites* mutant phenotype (van Eeden et al., 1996). Unchanged expression patterns of early somitic markers (*myoD*, *smad1*) confirmed this notion.

In a few exceptional cases, we have been able to raise homozygous mutants of the original sst^{t24295} allele to a later stage in life. Phenotypic analysis of larvae at different ages showed that the severity of bone defects increases over time, indicating that the gene affected in *sst* mutants is crucial for controlling proper ossification not only during embryogenesis, but also in late larval and adult stages. We suggest that *sst* activity is required throughout life to control osteogenesis, at least in axial skeletogenesis. This notion is supported by the late RA treatments we performed (17-20 dpf), which also resulted in axial over-ossification, indicating sensitivity to RA at late larval stages.

Hypomorphic and loss-of-function mutants for *cyp26b1*

Positional cloning of sst^{t24295} revealed two flanking markers enclosing the retinoic acid metabolizing gene *cyp26b1*, but no causative mutation could be found in this allele.

In order to identify additional alleles, we undertook a reverse genetic screen. We obtained two additional alleles of *sst*, both of which fail to complement the original sst^{t24295} allele. We focus in this study on sst^{sa0002}, which encodes a nonsense mutation in exon 1, predicted to change a lysine to a stop codon at position 46 (K46STOP; sst^{sa0002}) of the protein. As this will truncate the protein even N-terminal to the cytochrome P450 domain (at amino acid 50), we conclude that this allele encodes a loss-of-function allele.

When comparing the sst^{t24295} and the sst^{sa0002} allele, there are a number of noteworthy differences. First, all sst^{sa0002} mutants die shortly after hatching, whereas we have been able to raise very few sst^{t24295} homozygotes to late larval and adult stages. Second, when examining the head cartilage, sst^{t24295} does not show alterations when compared with wild-type siblings, whereas the sst^{sa0002} allele shows a protruding jaw and a reduced and misshapen ethmoid plate. Both lines of evidence suggest that sst^{t24295} is a hypomorph and that it represents a slightly weaker allele than sst^{sa0002}. The observed jaw phenotype is most likely the reason for early lethality in the strong alleles and correlates with the adult head skeleton phenotype that we find in the hypomorphic sst^{t24295} allele (Fig. 1C).

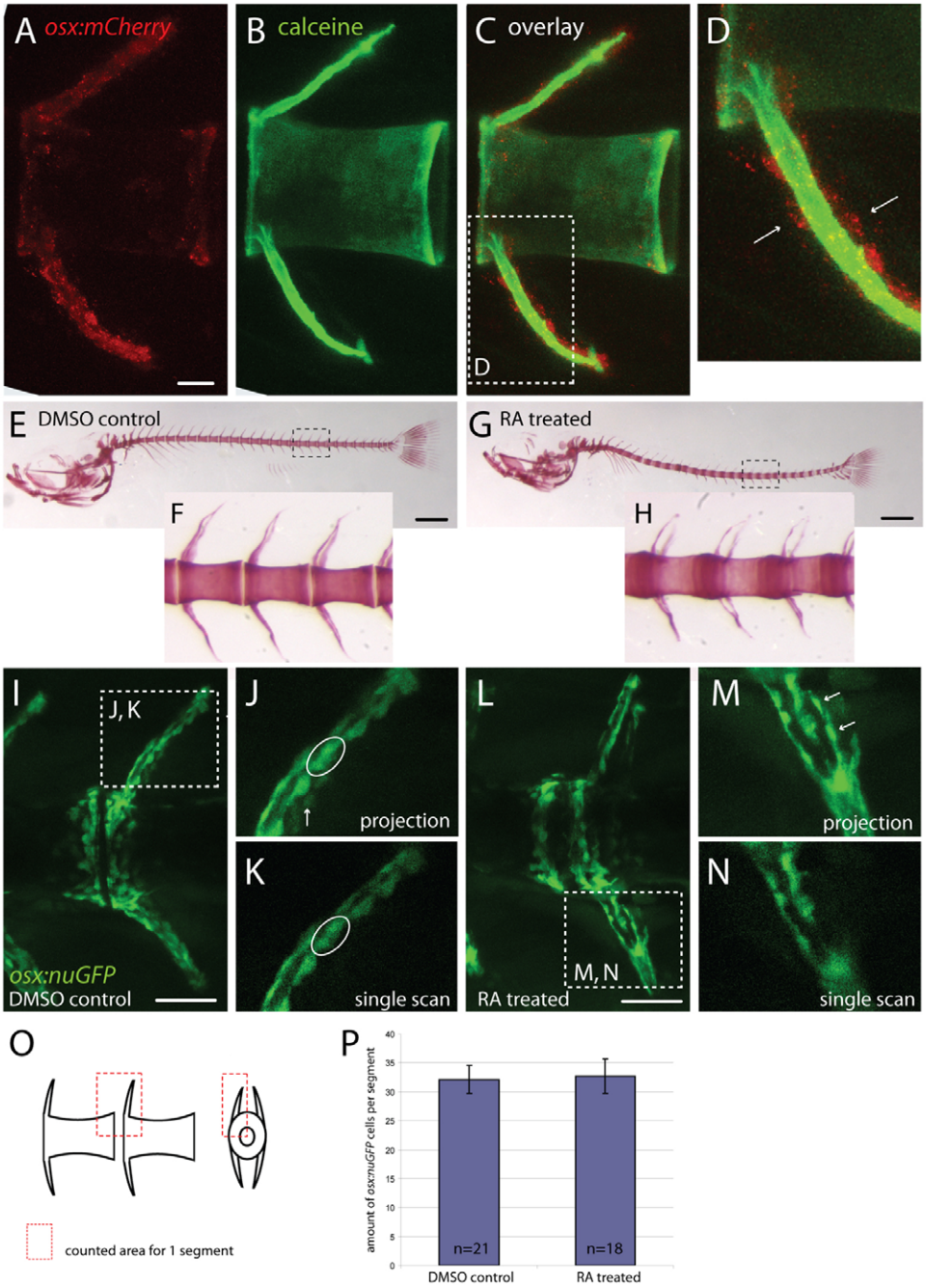

Fig. 6. RA treatment does not increase the number of *osterix:nuGFP*-positive osteoblasts in the centrum. (**A-D**) *osx:mCherry* expressing osteoblasts in a vertebra of a 20-day-old zebrafish. (A) *osx*-expressing cells are positioned around arches and at the anterior and posterior edges of each centrum, which is counterstained with calcein in B. Part of the overlay in C is shown in D. Osteoblasts are positioned distal to the produced bone matrix (examples are indicated with arrows). (**E-H**) Alizarin Red bone staining of 20-day-old zebrafish embryos treated with DMSO (E, enlargement in F) or 0.1 μM RA (G, enlargement in H) showing over-ossification of the vertebral column in RA-treated specimen. (**I-N**) *osx:nuGFP* expressing osteoblasts in 20-day-old zebrafish embryos treated with DMSO (I, enlargement in J) or 0.1 μM RA (L, enlargement in M). Single scans of one focal plane (K) were used to count cells. Cells indicated with arrows in projections (J,M) are not seen in single scans (K,N) as they belong to the arch at the opposite site. In single scans, cells can be distinguished from each other whereas in projections this is not always clear (encircled spot in J was resolved to represent two different cells in K). (M,N) High magnifications of a haemal arch that were actually not used for counting. (**O**) Schematic representation of vertebrae shows defined area in which cells were counted per segment. (**P**) Cell counts show no difference between DMSO controls and treated embryos in amount of *osx:nuGFP* positive osteoblasts. Scale bars: 25 μm in A-C; 500 μm in E,G; 50 μm in I,L.

In the original *stocksteif* allele, we also observe over-ossification of neural and haemal arches, whereas the other two *sst* alleles die too early to analyze arch formation. In mice, similar arch phenotypes can be observed by treatments with the Cyp26 inhibitor R115866, which results in over-ossification and fusion of arches of treated embryos (Laue et al., 2008). This suggests a conserved role for the function of Cyp26b1 among vertebrates.

Cyp26 mutants in mice

Cyp26b1 knockout mice die before the onset of vertebral deformities, owing to respiratory distress. Mutant mouse embryos, however, manifest reduced limbs (Yashiro et al., 2004). In fish, we do not observe phenotypes related to fin outgrowth, most probably because fin rays are evolutionary completely different from the digits of a mammalian limb (Grandel and Schulte-Merker, 1998).

Jaw phenotypes mimicking what we observe in both embryonic and adult *cyp26b1* mutants were not described in *Cyp26a1* mutant mice (Abu-Abed et al., 2001; Sakai et al., 2001). The *Cyp26a1* mouse phenotype therefore is clearly distinct from what we observe in zebrafish *cyp26b1* mutants. Moreover, expression patterns of both genes are also distinct from each other: compared with *Cyp26b1*, *Cyp26a1* expression is restricted to the extremities of the vertebral arches and ribs, and has not been detected in the pre-vertebrae regions (Abu-Abed et al., 2002).

We conclude that *stocksteif* manifests a novel phenotype, which allows new insight into the function of *cyp26b1* and retinoid signalling during vertebral ossification.

Retinoic acid treatment leads to axial over-ossification

Pharmacological treatments with either RA itself or the Cyp26 inhibitor R115866 completely phenocopy the *stocksteif* over-ossification phenotype, demonstrating a role for RA in ossification of the vertebral column. We propose that it is the regulation of Cyp26b1 activity, which defines local concentrations of RA within the vertebral area. Disruption of the gene or altered RA levels result in over-ossification along the vertebral column, most probably due to a local excess of RA within osteoblasts.

To support this notion, we examined the axial expression of *Cyp26b1* in zebrafish and mice. Localization of *Cyp26b1* transcripts in both species was found abutting the notochord, and comparison with zebrafish *twist* expression suggests that *Cyp26b1* is indeed expressed in sclerotome-derived cells of both teleosts and mammals. Furthermore, in both zebrafish and mice, we could clearly establish that *Cyp26b1* is expressed in cells that also express *osterix* (Fig. 3F-K; Fig. 4D-G). Therefore, we suggest that Cyp26b1 activity controls RA levels within osteoblasts, possibly setting up a boundary of low versus high RA levels between cells that express *Cyp26b1* and those that do not.

Evidence for two populations of osteoblasts

In zebrafish, we have never been able to detect *osterix* expression in the axial skeleton before arches appear, neither by in situ hybridization nor in the described transgenic lines. However, there is mineralized matrix present, as visualized by Alizarin Red or calcein staining, raising the issue of which cells are responsible for initial ossification of the very earliest centrum material. We suggest the existence of two types of osteoblasts: both are osteoblasts in the functional sense of secreting matrix that is then mineralized. However, one group does not express *osterix*, whereas the other group does. The latter group includes the osteoblasts of the future head skeleton, the vertebral arches and late-appearing osteoblasts at the anterior and posterior edges of the centra (Fig. 6A,C). The *osterix*-negative cells provide the initial material of the centrum body.

Further evidence for this hypothesis stems from Fleming et al. (Fleming et al., 2004), who were never able to detect osteoblasts in centrum bone matrix, whereas they could detect them in developing skull bones. It remains to be seen whether the *osterix*-negative cells are identical to cells of the notochord, which are postulated by Fleming et al. (Fleming et al., 2004) to initiate centrum formation.

Finally, it is interesting to note that osterix (*Sp7*)-null mutant mice are born with mineralized centra, whereas they lack almost all craniofacial bone elements (Nakashima et al., 2002). Although it is possible that centrum osteoblasts in mice express osterix, but do not require it for osteoblast function, it does point to a difference between centrum osteoblasts and all other osteoblasts.

Effects of retinoic acid on osteoblast activity

We considered three models that may explain why excess RA results in over-ossification: (1) RA causes ectopic bone formation by mis-positioning of osteoblasts; (2) RA causes an increase in osteoblast number; or (3) RA increases the activity of osteoblasts while not affecting their number.

To distinguish between these mechanisms, we made use of a zebrafish *osterix:nuGFP* transgenic reporter line, in order to directly visualize the response of mature osteoblasts to RA. We show that, upon RA treatment, *osterix*-positive osteoblasts do not change position, nor do they increase in number. We therefore favour the third model and suggest that osteoblasts increase their mineralization activity upon exposure to excess RA.

As at present there is no marker available for the putative *osterix*-negative osteoblasts in the centra, we are unable to assess whether RA also acts on this type of osteoblasts. It is noteworthy that skeletons of the adult hypomorphic *sst* mutants show over-ossification at precisely the sites where we do see *osterix* expression: anterior and posterior edges of the centra, as well as neural and haemal arches. Therefore, our results could be explained by postulating an increase in the activity of *osterix*-positive osteoblasts for the later aspects of the phenotype. However, we do consider it likely that RA also has an effect on *osterix*-negative osteoblasts, as the *sst* phenotype becomes apparent already at day 8 of development.

In the past, conflicting results have been reported about in vitro studies that have examined the effect of RA on mineralization. An increase in mineralization was reported (Skillington et al., 2002; Wang and Kirsch, 2002; Song et al., 2005; Yamashita et al., 2005; Malladi et al., 2006; Wan et al., 2007), whereas different studies show suppression of cell differentiation with a concomitant decrease in mineralization (Cohen-Tanugi and Forest, 1998; Iba et al., 2001) upon RA treatment of cultured cells. Here, we show in an in vivo setting that RA increases bone formation and suggest this to occur by an increased activity of osteoblasts. We have demonstrated that zebrafish offer an attractive model for performing genetic and pharmacological studies on osteoblasts, allowing in vivo observations and histological read-outs at the same time. In a field where the interpretation of in vitro and ex vivo experiments is inherently difficult, the use of an in vivo model that allows monitoring osteoblasts in real time will be highly beneficial.

A model for RA activity in axial skeletogenesis

We have shown that systemic treatment of larvae with RA produces phenotypes very similar to those of *cyp26b1* loss of function, even though one could speculate that mis-regulation of RA in axial osteoblasts causes a more spatially restricted increase in local RA levels, than exposing all cells to excess RA. We have incorporated all data presented in this manuscript in the following model.

In the wild-type situation, expression of Cyp26b1 protein within osteoblasts leads to lower RA levels within *cyp26b1*-positive cells (i.e. osteoblasts) than in neighbouring cells that do not express *cyp26b1* (i.e. non-osteoblasts). We propose that the juxtaposition of areas with low versus high RA levels is significant in maintaining *cyp26b1*-positive cells in a state in which they produce tightly controlled amounts of calcified matrix. Only when cells are exposed

to comparatively higher levels of RA, e.g. in *cyp26b1* mutants or after exposure to exogenous RA, will they then begin to produce an excess of calcified tissue.

In RA-treated embryos, all cells within the embryo experience high RA levels, and consequently there is no boundary between 'RA low' and 'RA high' regions. Accordingly, both *osterix*-negative osteoblasts within the body of the centrum and *osterix*-positive osteoblasts in the anterior and posterior regions of the centrum produce more matrix, leading to the observed over-ossification phenotype.

In loss-of-function *stocksteif* mutant embryos, RA levels are not lowered in osteoblasts (or only mildly lowered in the hypomorphic allele), again leading to increased osteoblast activity and resulting in the same events as just described for systemic RA exposure.

Conclusion

In summary, we have shown that regulation of RA levels and the tight control of Cyp26b1 activity are essential for regulation of skeletogenesis in zebrafish. Our data demonstrate a previously unappreciated role for RA and *cyp26b1* in osteogenesis of the vertebral column and provide novel insight into the regulation of bone formation.

The original *sst*^{t24295} allele was identified in the Tübingen 2000 Screen (F. Van Bebber, E. Busch-Nentwich, R. Dahm, O. Frank, H.-G. Fronhöfer, H. Geiger, D. Gilmour, S. Holly, J. Hooge, D. Jülich, H. Knaut, F. Maderspacher, H.-M. Maischein, C. Neumann, C. Nüsslein-Volhard, H. Roehl, U. Schönberger, C. Seiler, S. Sidi, M. Sonawane, A. Wehner, P. Erker, H. Habeck, U. Hagner, C. E. Hennen Kaps, A. Kirchner, T. Koblizek, U. Langheinrich, C. Loeschke, C. Metzger, R. Nordin, J. Odenthal, M. Pezzuti, K. Schlombs, J. deSantana-Stamm, T. Trowe, G. Vacun, B. Walderich, A. Walker and C. Weiler). Janssen Pharmaceutica kindly provided R115866. Ansa Wasim performed initial genomic mappings. Jeroen Bussmann performed BAC recombineering experiments. Identification of additional *sst* alleles by TILLING at the Hubrecht Institute and the Sanger Center would not have been possible without the enthusiastic help of (in alphabetical order) Ewart de Bruijn, Elisabeth Busch, Edwin Cuppen, Ross Kettleborough, and Derek Stemple. Kathrin Laue and Matthias Hammerschmidt shared results before publication. All members of S.S.-M.'s laboratory are acknowledged for discussions. S.S.-M. gratefully recognizes the support of the Smart Mix Programme of the Netherlands Ministry of Economic Affairs and the Netherlands Ministry of Education, Culture and Science. In part, this work was funded by ESA (15452/01/NL/SH) and an A*STAR BMRC grant (07/1/21/19/544) to C.W.

Supplementary material

Supplementary material for this article is available at
http://dev.biologists.org/cgi/content/full/135/22/3765/DC1

References

Abu-Abed, S., Dolle, P., Metzger, D., Beckett, B., Chambon, P. and Petkovich, M. (2001). The retinoic acid-metabolizing enzyme, CYP26A1, is essential for normal hindbrain patterning, vertebral identity, and development of posterior structures. *Genes Dev.* **15**, 226-240.

Abu-Abed, S., MacLean, G., Fraulob, V., Chambon, P., Petkovich, M. and Dolle, P. (2002). Differential expression of the retinoic acid-metabolizing enzymes CYP26A1 and CYP26B1 during murine organogenesis. *Mech. Dev.* **110**, 173-177.

Avaron, F., Hoffman, L., Guay, D. and Akimenko, M. A. (2006). Characterization of two new zebrafish members of the hedgehog family: atypical expression of a zebrafish indian hedgehog gene in skeletal elements of both endochondral and dermal origins. *Dev. Dyn.* **235**, 478-489.

Bowles, J., Knight, D., Smith, C., Wilhelm, D., Richman, J., Mamiya, S., Yashiro, K., Chawengsaksophak, K., Wilson, M. J., Rossant, J., Hamada, H. and Koopman, P. (2006). Retinoid signaling determines germ cell fate in mice. *Science* **312**, 596-600.

Cohen-Tanugi, A. and Forest, N. (1998). Retinoic acid suppresses the osteogenic differentiation capacity of murine osteoblast-like 3/A/1D-1M cell cultures. *Differentiation* **63**, 115-123.

Ekanayake, S. and Hall, B. K. (1987). The development of acellularity of the vertebral bone of the Japanese medaka, Oryzias latipes (Teleostei; Cyprinidontidae). *J. Morphol.* **193**, 253-261.

Emoto, Y., Wada, H., Okamoto, H., Kudo, A. and Imai, Y. (2005). Retinoic acid-metabolizing enzyme Cyp26a1 is essential for determining territories of hindbrain and spinal cord in zebrafish. *Dev. Biol.* **278**, 415-427.

Feldkamp, L. A., Davis, L. C. and Kress, J. W. (1984). Practical cone-beam algorithm. *J. Opt. Soc. Am. A* **1**, 612-619.

Fleming, A., Keynes, R. and Tannahill, D. (2004). A central role for the notochord in vertebral patterning. *Development* **131**, 873-880.

Grandel, H. and Schulte-Merker, S. (1998). The development of the paired fins in the zebrafish (Danio rerio). *Mech. Dev.* **79**, 99-120.

Gu, X., Xu, F., Wang, X., Gao, X. and Zhao, Q. (2005). Molecular cloning and expression of a novel CYP26 gene (cyp26d1) during zebrafish early development. *Gene Expr. Patterns* **5**, 733-739.

Hernandez, R. E., Putzke, A. P., Myers, J. P., Margaretha, L. and Moens, C. B. (2007). Cyp26 enzymes generate the retinoic acid response pattern necessary for hindbrain development. *Development* **134**, 177-187.

Iba, K., Chiba, H., Yamashita, T., Ishii, S. and Sawada, N. (2001). Phase-independent inhibition by retinoic acid of mineralization correlated with loss of tetranectin expression in a human osteoblastic cell line. *Cell Struct. Funct.* **26**, 227-233.

Inohaya, K., Takano, Y. and Kudo, A. (2007). The teleost intervertebral region acts as a growth center of the centrum: in vivo visualization of osteoblasts and their progenitors in transgenic fish. *Dev. Dyn.* **236**, 3031-3046.

Kawakami, K., Koga, A., Hori, H. and Shima, A. (1998). Excision of the tol2 transposable element of the medaka fish, Oryzias latipes, in zebrafish, Danio rerio. *Gene* **225**, 17-22.

Keegan, B. R., Feldman, J. L., Begemann, G., Ingham, P. W. and Yelon, D. (2005). Retinoic acid signaling restricts the cardiac progenitor pool. *Science* **307**, 247-249.

Kimura, Y., Okamura, Y. and Higashijima, S. (2006). alx, a zebrafish homolog of Chx10, marks ipsilateral descending excitatory interneurons that participate in the regulation of spinal locomotor circuits. *J. Neurosci.* **26**, 5684-5697.

Laue, K., Jänicke, M., Plaster, N., Sonntag, C. and Hammerschmidt, M. (2008). Restriction of retinoic acid activity by Cyp26b1 is required for proper timing and patterning of osteogenesis during zebrafish development. *Development* **135**, 3775-3787.

MacLean, G., Abu-Abed, S., Dolle, P., Tahayato, A., Chambon, P. and Petkovich, M. (2001). Cloning of a novel retinoic-acid metabolizing cytochrome P450, Cyp26B1, and comparative expression analysis with Cyp26A1 during early murine development. *Mech. Dev.* **107**, 195-201.

Maden, M. (2002). Retinoid signalling in the development of the central nervous system. *Nat. Rev. Neurosci.* **3**, 843-853.

Malladi, P., Xu, Y., Yang, G. P. and Longaker, M. T. (2006). Functions of vitamin D, retinoic acid, and dexamethasone in mouse adipose-derived mesenchymal cells. *Tissue Eng.* **12**, 2031-2040.

Moorman, A. F., Houweling, A. C., de Boer, P. A. and Christoffels, V. M. (2001). Sensitive nonradioactive detection of mRNA in tissue sections: novel application of the whole-mount in situ hybridization protocol. *J. Histochem. Cytochem.* **49**, 1-8.

Morin-Kensicki, E. M. and Eisen, J. S. (1997). Sclerotome development and peripheral nervous system segmentation in embryonic zebrafish. *Development* **124**, 159-167.

Nakashima, K., Zhou, X., Kunkel, G., Zhang, Z., Deng, J. M., Behringer, R. R. and de Crombrugghe, B. (2002). The novel zinc finger-containing transcription factor osterix is required for osteoblast differentiation and bone formation. *Cell* **108**, 17-29.

Nelson, D. R. (1999). A second CYP26 P450 in humans and zebrafish: CYP26B1. *Arch. Biochem. Biophys.* **371**, 345-347.

Reijntjes, S., Rodaway, A. and Maden, M. (2007). The retinoic acid metabolising gene, CYP26B1, patterns the cartilaginous cranial neural crest in zebrafish. *Int. J. Dev. Biol.* **51**, 351-360.

Rembold, M., Lahiri, K., Foulkes, N. S. and Wittbrodt, J. (2006). Transgenesis in fish: efficient selection of transgenic fish by co-injection with a fluorescent reporter construct. *Nat. Protocols* **1**, 1133-1139.

Renn, J., Schaedel, M., Volff, J. N., Goerlich, R., Schartl, M. and Winkler, C. (2006). Dynamic expression of sparc precedes formation of skeletal elements in the Medaka (Oryzias latipes). *Gene* **372**, 208-218.

Ross, S. A., McCaffery, P. J., Drager, U. C. and De Luca, L. M. (2000). Retinoids in embryonal development. *Physiol Rev.* **80**, 1021-1054.

Sakai, Y., Meno, C., Fujii, H., Nishino, J., Shiratori, H., Saijoh, Y., Rossant, J. and Hamada, H. (2001). The retinoic acid-inactivating enzyme CYP26 is essential for establishing an uneven distribution of retinoic acid along the anterio-posterior axis within the mouse embryo. *Genes Dev.* **15**, 213-225.

Schulte-Merker, S. (2002). Looking at embryos. In *Zebrafish, A Practical Approach* (ed. C. Nüsslein-Volhard and R. Dahm), pp. 41-43. New York: Oxford University Press.

Skillington, J., Choy, L. and Derynck, R. (2002). Bone morphogenetic protein and retinoic acid signaling cooperate to induce osteoblast differentiation of preadipocytes. *J. Cell Biol.* **159**, 135-146.

Song, H. M., Nacamuli, R. P., Xia, W., Bari, A. S., Shi, Y. Y., Fang, T. D. and Longaker, M. T. (2005). High-dose retinoic acid modulates rat calvarial osteoblast biology. *J. Cell Physiol.* **202**, 255-262.

van Eeden, F. J., Granato, M., Schach, U., Brand, M., Furutani-Seiki, M., Haffter, P., Hammerschmidt, M., Heisenberg, C. P., Jiang, Y. J., Kane, D. A.

et al. (1996). Mutations affecting somite formation and patterning in the zebrafish, Danio rerio. *Development* **123**, 153-164.
Waarsing, J. H., Day, J. S. and Weinans, H. (2004). An improved segmentation method for in vivo microCT imaging. *J. Bone Miner. Res.* **19**, 1640-1650.
Walker, M. B. and Kimmel, C. B. (2007). A two-color acid-free cartilage and bone stain for zebrafish larvae. *Biotech. Histochem.* **82**, 23-28.
Wan, D. C., Siedhoff, M. T., Kwan, M. D., Nacamuli, R. P., Wu, B. M. and Longaker, M. T. (2007). Refining retinoic acid stimulation for osteogenic differentiation of murine adipose-derived adult stromal cells. *Tissue Eng.* **13**, 1623-1631.
Wang, W. and Kirsch, T. (2002). Retinoic acid stimulates annexin-mediated growth plate chondrocyte mineralization. *J. Cell Biol.* **157**, 1061-1069.
White, J. A., Guo, Y. D., Baetz, K., Beckett-Jones, B., Bonasoro, J., Hsu, K. E., Dilworth, F. J., Jones, G. and Petkovich, M. (1996). Identification of the retinoic acid-inducible all-trans-retinoic acid 4-hydroxylase. *J. Biol. Chem.* **271**, 29922-29927.
White, J. A., Ramshaw, H., Taimi, M., Stangle, W., Zhang, A., Everingham, S., Creighton, S., Tam, S. P., Jones, G. and Petkovich, M. (2000). Identification of the human cytochrome P450, P450RAI-2, which is predominantly expressed in the adult cerebellum and is responsible for all-trans-retinoic acid metabolism. *Proc. Natl. Acad. Sci. USA* **97**, 6403-6408.
White, R. J., Nie, Q., Lander, A. D. and Schilling, T. F. (2007). Complex regulation of cyp26a1 creates a robust retinoic acid gradient in the zebrafish embryo. *PLoS Biol.* **5**, e304.
Wienholds, E., Schulte-Merker, S., Walderich, B. and Plasterk, R. H. (2002). Target-selected inactivation of the zebrafish rag1 gene. *Science* **297**, 99-102.
Yamashita, A., Takada, T., Narita, J., Yamamoto, G. and Torii, R. (2005). Osteoblastic differentiation of monkey embryonic stem cells in vitro. *Cloning Stem Cells* **7**, 232-237.
Yashiro, K., Zhao, X., Uehara, M., Yamashita, K., Nishijima, M., Nishino, J., Saijoh, Y., Sakai, Y. and Hamada, H. (2004). Regulation of retinoic acid distribution is required for proximodistal patterning and outgrowth of the developing mouse limb. *Dev. Cell* **6**, 411-422.
Zhao, Q., Dobbs-McAuliffe, B. and Linney, E. (2005). Expression of cyp26b1 during zebrafish early development. *Gene Expr. Patterns* **5**, 363-369.